

Simultaneous polarization separation and switching for 100-Gbps DP-QPSK signals in backbone networks

Yu-Long Su(苏玉龙), Huan Feng(冯欢), Hui Hu(胡辉), Wei Wang(汪伟),Tao Duan(段弢), Yi-Shan Wang(王屹山), Jin-Hai Si(司金海),Xiao-Ping Xie(谢小平), He-Ning Yang(杨合宁), and Xin-Ning Huang(黄新宁)

Citation: Chin. Phys. B . 2019, 28(2): 024216. **doi:** 10.1088/1674-1056/28/2/024216
Journal homepage: http://cpb.iphy.ac.cn; http://iopscience.iop.org/cpb

What follows is a list of articles you may be interested in

Polarization-based range-gated imaging in birefringent medium:Effect of size parameter

Heng Tian(田恒), Jing-Ping Zhu(朱京平), Shu-Wen Tan(谭树文), Jing-Jing Tian(田晶晶), Yun-Yao Zhang(张云尧), Xun Hou(侯洵)

Chin. Phys. B . 2018, 27(12): 124203. **doi:** 10.1088/1674-1056/27/12/124203

Three-dimensional modulations on the states of polarization of light fields

Peng Li(李鹏), Dongjing Wu(吴东京), Sheng Liu(刘圣), Yi Zhang(章毅), Xuyue Guo(郭旭岳), Shuxia Qi(齐淑霞), Yu Li(李渝), Jianlin Zhao(赵建林)

Chin. Phys. B . 2018, 27(11): 114201. **doi:** 10.1088/1674-1056/27/11/114201

β-BaB_2O_4 with special cut-angle applied to single crystal cascaded third-harmonic generation

Hong-Kai Ren(任宏凯), Hong-Wei Qi(亓宏伟), Zheng-Ping Wang(王正平), Zhi-Xin Wu(吴志心), Meng-Xia Wang(王梦霞), Yu-Xiang Sun(孙玉祥), Xun Sun(孙洵), Xin-Guang Xu(许心光)

Chin. Phys. B . 2018, 27(11): 114202. **doi:** 10.1088/1674-1056/27/11/114202

Silicon nanophotonics for on-chip light manipulation

Jingshu Guo(郭敬书), Daoxin Dai(戴道锌)

Chin. Phys. B . 2018, 27(10): 104208. **doi:** 10.1088/1674-1056/27/10/104208

Wideband linear-to-circular polarization conversion realized by a transmissive anisotropic metasurface

Bao-Qin Lin(林宝勤), Jian-Xin Guo(郭建新), Bai-Gang Huang(黄百钢), Lin-Bo Fang(方林波), Peng Chu(储鹏), Xiang-Wen Liu(刘湘雯)

Chin. Phys. B . 2018, 27(5): 054204. **doi:** 10.1088/1674-1056/27/5/054204

Simultaneous polarization separation and switching for 100-Gbps DP-QPSK signals in backbone networks*

Yu-Long Su(苏玉龙)[1,2,3], Huan Feng(冯欢)[1,3], Hui Hu(胡辉)[1,3], Wei Wang(汪伟)[1,3], Tao Duan(段弢)[1,3], Yi-Shan Wang(王屹山)[1], Jin-Hai Si(司金海)[2], Xiao-Ping Xie(谢小平)[1], He-Ning Yang(杨合宁)[1,2,3], and Xin-Ning Huang(黄新宁)[1,3,†]

[1] *State Key Laboratory of Transient Optics and Photonics, Xi'an Institute of Optics and Precision Mechanics, Chinese Academy of Sciences, Xi'an* 710119, *China*

[2] *Key Laboratory for Physical Electronics and Devices of the Ministry of Education and Shaanxi Key Laboratory of Information Photonic Technique, School of Electronic and Information Engineering, Xi'an Jiaotong University, Xi'an* 710049, *China*

[3] *University of Chinese Academy of Sciences, Beijing* 100049, *China*

(Received 20 November 2018; revised manuscript received 23 December 2018; published online 25 January 2019)

We propose a novel scheme of simultaneous polarization separation and switching, based on the orthogonally-polarized four-wave mixing (FWM) effect, for ultra-high-speed polarization multiplexing (Pol-MUX) fiber networks such as 100-Gbps and 400-Gbps backbone networks. We use theoretical and experimental analysis of the vector theory of FWM to successfully achieve polarization separation and all-optical switching by utilizing a 100-Gbps dual polarization-quadrature phase shift keying (DP-QPSK) signal and two orthogonally-polarized pumps. Both of the polarization-separated QPSK signals have clear constellation diagrams, with root mean square (RMS) error vector magnitudes (EVMs) of 14.32% and 14.11% respectively. The wavelengths of idlers can be created at 30 different wavelengths, which are consistent with International Telecommunication Union-Telecommunication (ITU-T) wavelengths, by flexibly changing the wavelength of the pump light. Moreover, the idlers that have distinct wavelengths have power distributed in a range from −10 dBm to −15 dBm, which can support error-free transmission. The power penaltyis 5 dB lower than that of back-to-back (BTB) signal for both the X- and Y-polarization components measured at a bit error ratio (BER) of 3.8×10^{-3}. Our experimental results indicate that this scheme has promising applications in future backbone networks.

Keywords: polarization separation and switching, four-wave mixing, orthogonal polarization, 100-Gbps dual polarization-quadrature phase shift keying

PACS: 42.25.Ja, 42.65.Ky, 42.79.Sz **DOI:** 10.1088/1674-1056/28/2/024216

1. Introduction

The rapidly developing importance of information in the modern world means that there is a perpetual demand for increased bandwidths of fiber backbone networks; most of these networks are installed on a commercial basis, which mainly consist of 10-Gbps and 40-Gbps channels.[1–3] The coherent 100-Gbps[4] technology has been used maturely in backbone networks, and is now becoming widely available in long-reach and long-haul links. The development of the next generation of 400-Gbps[5] transmission has also been the subject of extensive research in many countries.

Polarization multiplexing (Pol-MUX)[6–12] technology is a simple and practical approach currently used to achieve long-haul transmission; it can efficiently utilize the available spectra in the 100-, 200-, and 400-Gbps backbone networks. The Pol-MUX modulates two independent datasets, each on two orthogonal polarization states, at a single wavelength. This can double the communication capacity. Specific applications of Pol-MUX include 100-Gbps dual polarization-quadrature phase shift keying (DP-QPSK), 200-Gbps dual polarization 16-ary quadrature amplitude (DP-16-QAM), and 400-Gbps DP-64-QAM transmissions.[13–15]

Moreover, the simultaneous polarization separation and the switching of Pol-MUX signals between different nodes are particularly important parts of a fiber network; data exchange often occurs in one of the polarization states of a Pol-MUX signal. In previous studies, the optical signal carrying traffic undergoes an optical–electronic–optical (OEO) conversion at every routing node. The traditional method of carrying out one polarization state signal switching from node A to node B is based on an electrical switching chip[16,17] as shown in Fig. 1. Here, we assume that two node signals, S_1 and S_2, go to nodes B_{n-1} and B_{n-2} to illustrate the process of polarization separation and switching. First, S_1 and S_2 are loaded onto two orthogonal polarization states to form an optical Pol-MUX signal; they reach the receiver through the fiber. Second, the Pol-MUX signal is demodulated by coherent detection and digital signal processing (DSP) to recover the electrical signals of S_1 and S_2.[18,19] Finally, the two signals are switched to nodes B_{n-1} and B_n via the electrical switching and E/O con-

*Project supported by the National Key Research and Development Program of China (Grant No. 2017YFC0803900) and the National Natural Science Foundation of China (Grant No. 9163801).

†Corresponding author. E-mail: realkeo@126.com

© 2019 Chinese Physical Society and IOP Publishing Ltd

version. However, this method has some significant shortcomings as indicated below. It is not suitable for ultra-high speed Pol-MUX signals (such as 100-Gbps DP-QPSK) due to the limited data rate of the commercial electrical switching chips (serial data rate up to 10 Gbps), and complicated signal demodulation and digital algorithm processing is required for the OEO conversion, which gives the network a large delay and a low efficiency.

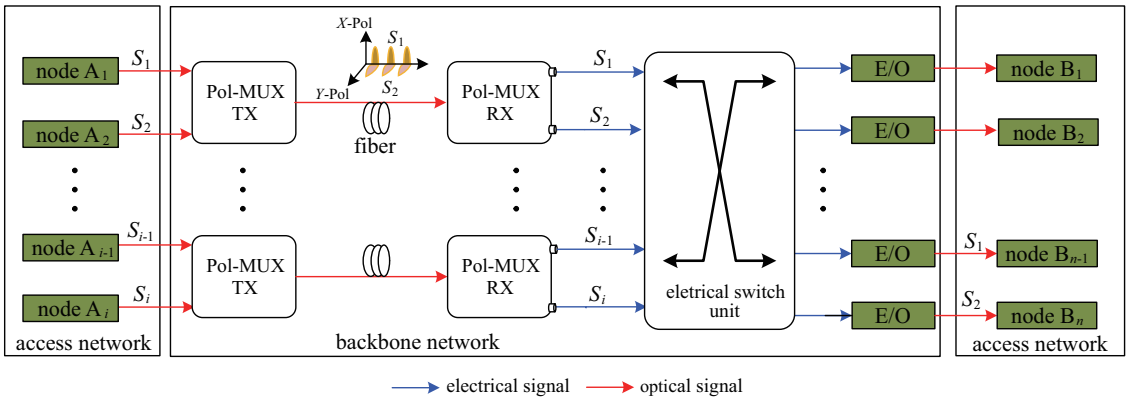


Fig. 1. Schematic diagram of a traditional electrical switching process.

An effective solution to handle an ultra-high data rate, however, is to make use of the optical switching[20,21] technology, which can achieve higher bandwidth, lower power consumption, and lower operation cost, than the traditional methods. Optical switching uses optical cross-connects and reconfigurable optical add/drop multiplexers (ROADMs). These optical switches include optical microelectromechanical system (MEMS)-based switching, thermal optical switching, electro-optic switching, and nonlinear optical switching. The nonlinear optical switches perform switching functions by using the intensity-dependent nonlinear optic effect (which is ultrafast) in the nonlinear fiber or waveguide, such as two-photon absorption and the Kerr[22,23] effect. This induces the optical phenomena of four-wave mixing (FWM) and cross phase modulation (XPM). Of these nonlinear effects, the FWM[24–28] most promises to realize multi-channel wavelength conversion and polarization separation for Pol-MUX signals in optical networks. FWM is a third-order nonlinear effect, which is transparent to the modulation format and data rate and compatible with DP-QPSK and DP-16QAM.[29,30]

In this paper, we propose a novel scheme for the all optical polarization separation and switching of a 100-Gbps DP-QPSK signal, which has potential applications in future backbone networks as shown in Fig. 2, severing as a replacement for electrical switching. We separate the two orthogonal polarization states of the 100-Gbps DP-QPSK signal into two independent channels with different wavelengths by using the orthogonally-polarized FWM effect. Both of these separated signals with orthogonal polarization states have clear constellation diagrams with root mean square (RMS) error vector magnitudes (EVMs) of 14.32% and 14.11%, respectively. The idlers can be created at 30 different wavelengths, consistent with the International Telecommunication Union-Telecommunication (ITU-T) wavelengths, by flexibly changing the wavelength of the pump light. In addition, these idlers with distinct wavelengths exhibit power distributed in a range from -10 dBm to -15 dBm after a 150-km transmission, supporting an error-free transmission. The measured power penalty is 5 dB lower than that of the back-to-back (BTB) signal for both the X- and Y-polarization components at a bit error ratio (BER) of 3.8×10^{-3}.

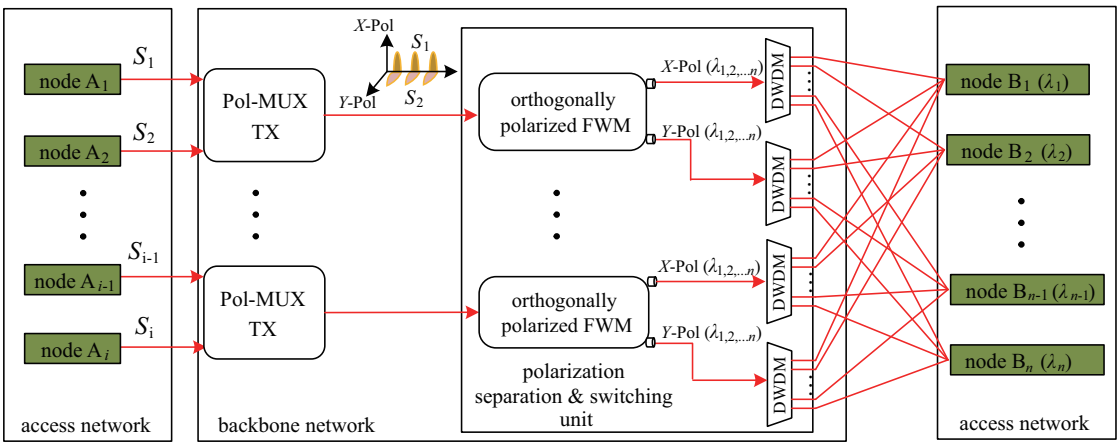


Fig. 2. Schematic diagram of proposed simultaneous polarization separation switching process for Pol-MUX signal in a backbone network.

2. Principle of orthogonally-polarized four wave mixing

The principles of polarization separation and simultaneous switching can be explained by using the FWM process. Firstly, we investigate the physical mechanism of wavelength conversion by using two pumps and a Pol-MUX signal configuration, through using a highly-nonlinear fiber (HNLF). We induce the basic FWM spectra at the three frequencies shown in Fig. 3(a), where P_1 and P_2 represent two pumps with orthogonal polarization states. In the FWM process, there are about seven idler light beams generated at the three mixing frequencies. Here, we mainly consider the three idler light beams denoted as idler-1, idler-2, and idler-3, which are located at the frequencies given by

$$\begin{aligned}\omega_{\text{idler}-1} &= 2\omega_{p1} - \omega_s,\\ \omega_{\text{idler}-2} &= 2\omega_{p2} - \omega_s,\\ \omega_{\text{idler}-3} &= \omega_{p1} + \omega_{p2} - \omega_s,\end{aligned} \tag{1}$$

where ω_{p1}, ω_{p2}, and ω_s are the frequencies of the P_1, P_2, and Pol-MUX signals, respectively. Idler-6 and idler-7 are similar to idler-1 and idler-2 because they are all composed of two frequencies; idler-4 and idler-5 are similar to idler-3 in the same fashion. Therefore, the theoretical analyses of idler-1, idler-2, and idler-3 are suitable for other similar idlers.

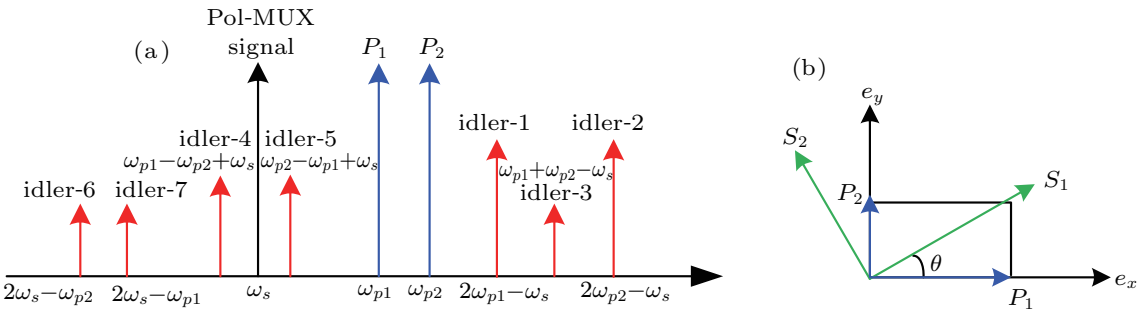


Fig. 3. (a) Schematic diagram of FWM spectrum induced by two pumps and a Pol-MUX signal, and (b) polarization directions of the two pumps and the Pol-MUX signal.

Here, we assume that the Pol-MUX signal is comprised of the orthogonally-polarized signals S_1 and S_2, and that signal S_1 has an initial angle θ with respect to the pump P_1 as shown in Fig. 3(b).

We express the electric field vectors of the two orthogonally polarized pumps ($\boldsymbol{E}_{p1}$ and $\boldsymbol{E}_{p2}$) and the Pol-MUX signal ($\boldsymbol{E}_s$) as follows:

$$\boldsymbol{E}_{p1} = A_{p1}\exp(\mathrm{j}(\omega_{p1}t - \varphi_{p1}))e_x, \tag{2}$$

$$\boldsymbol{E}_{p2} = A_{p2}\exp(\mathrm{j}(\omega_{p2}t - \varphi_{p2}))e_y, \tag{3}$$

$$\begin{aligned}\boldsymbol{E}_s = {} & \exp(\mathrm{j}(\omega_s t - \varphi_s))[(A_{s1}\cos(\theta) + A_{s2}\cos(90+\theta))]e_x\\ & + \exp(\mathrm{j}(\omega_s t - \varphi_s))[A_{s1}\sin(\theta) + A_{s2}\cos(\theta)]e_y.\end{aligned} \tag{4}$$

Here, A_{p1} and A_{p2} are the amplitudes, ω_{p1} and ω_{p2} are the frequencies, and φ_{p1} and φ_{p2} are the phases of the pumps P_1 and P_2 respectively; A_{s1} and A_{s2} represent the amplitudes of the signals S_1 and S_2, respectively, which are the orthogonal components of the Pol-MUX signal; ω_s and φ_s are the frequency and phase of the Pol-MUX signal, respectively. The generated electric field vectors of three idlers are given by[20–23]

$$\boldsymbol{E}_{\text{idler}-1} = \eta_2(\boldsymbol{E}_{p1}\cdot\boldsymbol{E}_s^*)\boldsymbol{E}_{p1}, \tag{5}$$

$$\boldsymbol{E}_{\text{idler}-2} = \eta_3(\boldsymbol{E}_{p2}\cdot\boldsymbol{E}_s^*)\boldsymbol{E}_{p2}, \tag{6}$$

$$\begin{aligned}\boldsymbol{E}_{\text{idler}-3} = {} & \eta_1(\boldsymbol{E}_{p1}\cdot\boldsymbol{E}_s^*)\boldsymbol{E}_{p2} + \eta_2(\boldsymbol{E}_{p2}\cdot\boldsymbol{E}_s^*)\boldsymbol{E}_{p1}\\ & + \eta_3(\boldsymbol{E}_{p2}\cdot\boldsymbol{E}_{p1})\boldsymbol{E}_s^*,\end{aligned} \tag{7}$$

where η_1, η_2, and η_3 are the conversion efficiencies of the FWM processes. These conversion efficiencies are determined by the incident power, frequency, and dispersion of the HNLF. The dot product of two field vectors ('·') is the inner product that represents their beating operation. When the mixing frequency polarization states are orthogonally polarized, the dot product will be zero; it will be at its maximum when they are parallel polarized. Substituting Eqs. (2)–(4) into Eqs. (5)–(7), respectively, the three idlers' electric fields can be expressed as,

$$\begin{aligned}\boldsymbol{E}_{\text{idler}-1} = {} & \eta_2 A_{p1}\exp(\mathrm{j}(2\omega_{p1} - \omega_s)t - (2\varphi_{p1} - \varphi_s))\\ & \times[(A_{s1}\cos(\theta) + A_{s2}\cos(90+\theta))]e_x,\end{aligned} \tag{8}$$

$$\begin{aligned}\boldsymbol{E}_{\text{idler}-2} = {} & \eta_1 A_{p2}\exp(\mathrm{j}(2\omega_{p2} - \omega_s)t - (2\varphi_{p2} - \varphi_s))\\ & \times[(A_{s1}\sin(\theta) + A_{s2}\cos(\theta))]e_y,\end{aligned} \tag{9}$$

$$\begin{aligned}\boldsymbol{E}_{\text{idler}-3} = {} & A_{p1}A_{p2}\exp(\mathrm{j}(\omega_{p1} + \omega_{p2} - \omega_s)t\\ & - (\varphi_{p1} + \varphi_{p2} - \varphi_s))(\eta_1 + \eta_2)\\ & \times[(A_{s1}\cos(\theta) + A_{s2}\cos(90+\theta))]e_x\\ & + \eta_1 A_{p1}A_{p2}\exp(\mathrm{j}(\omega_{p1} + \omega_{p2} - \omega_s)t\\ & - (\varphi_{p1} + \varphi_{p2} - \varphi_s))\\ & \times[(A_{s1}\sin(\theta) + A_{s2}\cos(\theta))]e_y.\end{aligned} \tag{10}$$

When $\theta = 0^\circ$, the component $A_{s2}\cos(90+\theta)$ in Eq. (9) will be zero, and the component $A_{s1}\cos(\theta)$ will reach its maximum value. This means that the electric field $\boldsymbol{E}_{\text{idler}-1}$ only contains the full information about S_1. Similarly, $\boldsymbol{E}_{\text{idler}-2}$ only contains the full information about S_2. The information about $\boldsymbol{E}_{\text{idler}-1}$ and the information about $\boldsymbol{E}_{\text{idler}-2}$ are interchanged

when $\theta = 90°$. However, $\boldsymbol{E}_{\text{idler}-3}$ has the mixed components of A_{s1} and A_{s2}, no matter whether θ is 0° or 90°, meaning that $\boldsymbol{E}_{\text{idler}-3}$ cannot be used as the result of the polarization separation.

It can be seen from the above theoretical analysis that the polarization separation of the Pol-MUX signal can be achieved by using two orthogonally-polarized pumps and the same polarization direction Pol-MUX signal to construct the FWM effect, and then choosing idlers at frequencies of $2\omega_{p1} - \omega_s$ and $2\omega_{p2} - \omega_s$ as polarization separation results.

3. Experimental setup

Figure 4 shows our experimental configuration, based on the polarization separation and switching of a 100-Gbps DP-QPSK in a fiber network. It consists of a 100-Gbps DP-QPSK transmitter, a polarization separation, a switching unit, and two node receivers. The 100-Gbps DP-QPSK transmitter contains an external cavity laser (ECL, Neophotonics TTX1995), a 25-GHz $LiNbO_3$ IQ modulator (EOSPACE, IQ-0D6 K-25-PFA-PFA-LV), an arbitrary waveform generator (AWG, Tektronix AWG70002) with a sampling rate of 50 GS/s, and a polarization multiplexer (Pol-MUX unit). At the transmitter, continuous-wave light (∼ 20-kHz linewidth) generated from the ECL at 1548.52 nm with power of 18 dBm, is modulated by the IQ modulator. The IQ modulator is driven by two independent 25-Gbps electrical data signals from the AWG, to form a 25-GBd QPSK signal. The two data patterns are $2^{15} - 1$ pseudo-random bit sequence (PRBS) data streams, with a 20-bit delay between the two data patterns. Simultaneously, an automatic bias control (ABC) board provides three precise voltages to maintain the IQ modulator operating at a normal point, achieving the optimal modulation effect and providing long-term stability. A Pol-MUX emulator is used to generate a 25-GBd (100 Gbps) DP-QPSK signal to double the data rate, after which the signal passes through a variable optical attenuation (VOA, Santec OVA-650) to simulate fiber losses. The Pol-MUX emulator is shown in Fig. 5. The generated QPSK signal is divided into two paths by a polarization maintaining optical coupler (PM-OC), one of which is delayed by 800 ps and the other QPSK signal is attenuated by VOA to balance the power of the two paths. A polarization beam combiner (PBC) is employed to combine the two paths to form a DP-QPSK signal. A low noise erbium doped fiber amplifier (EDFA, Keopsys CEFA-C-HG-SM-50-M201-FA-FA) with noise figure of 3.7 dB is used to compensate for the power loss, and a Gaussian filter (Finisar, Waveshaper 4000) is used to filter out the noise to improve the optical signal-to-noise ratio (OSNR).

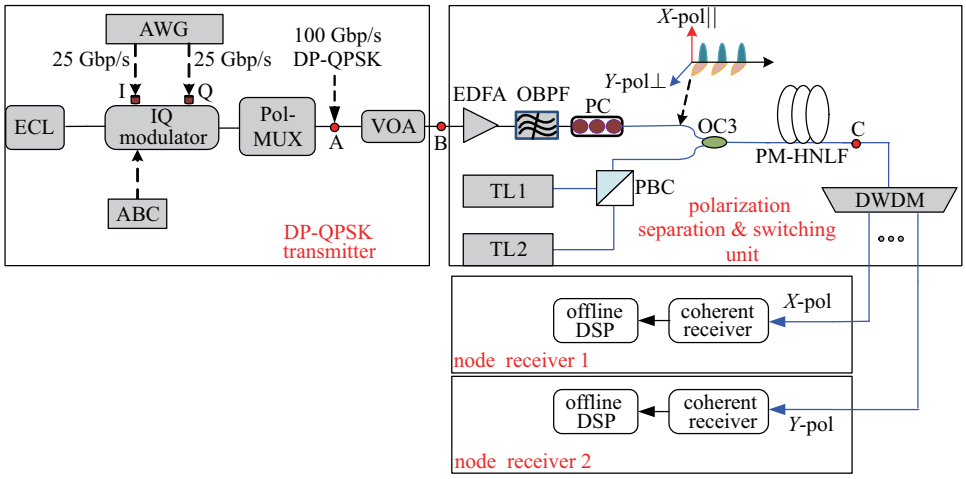


Fig. 4. Experimental configuration diagram of the 100-Gbps DP-QPSK polarization separation and switching.

In the FWM-based polarization separation and switching unit, the attenuated signal is amplified by an EDFA (Amonics AEDFA-PA-35) with a gain of > 30 dB and a noise figure of < 3.7 dB. It is then filtered by a Gaussian optical band pass filter (OBPF) with a 3-dB bandwidth of 0.42 nm. Two narrow-linewidth tunable lasers (TL 1 and TL 2, Emcore TTX1995 with a linewidth of ∼ 20 kHz) are provided and denoted as CW pump 1 and pump 2; they are combined by a PBC. The X-polarization (X-Pol) and Y-polarization (Y-Pol) state of the DP-QPSK signal are precisely rotated by a three-wave-plate adjustable polarization controller (PC, Thorlabs, PC-FFB-1550) to align them with the two pumps. It should be noted that we use the PC to replace the polarization tracking device[31–33] for the convenience of the experiment. The mixed signals are combined by a polarization maintaining coupler, and then launched into a 500-m-long HNLF with a nonlinearity coefficient of 11.5 $\text{W}^{-1}\cdot\text{km}^{-1}$ and a chromatic dispersion of -1.5 ps/(nm · km) at 1550 nm in wavelength. Furthermore, with the polarization separation results, we filter the idlers out from the FWM spectrum by using the customized 50-GHz spacing dense wavelength-division multiplexing (DWDM) module. We then sent them to the two

wavelength-addressed node receivers, which experience the coherent detection and offline digital signal process to recover the signals.

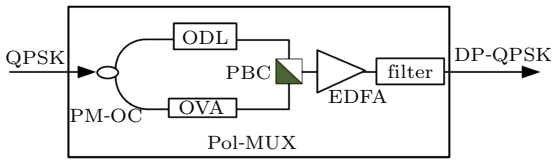


Fig. 5. Pol-MUX emulator configuration.

4. Results and discussion

Figure 6(a) depicts the transmitted a 100-Gbps DP-QPSK optical spectrum. It has an OSNR of 64 dB as measured by the optical spectrum analyzer (YOKOGAWA, AQ6370). Figure 6(b) shows the DP-QPSK signal eye diagram, which exhibits a clear profile measured by the digital sampling oscilloscope (DSO, Tektronix, TDS8200) together with a 50-GHz photodetector (XPDV2020R, U^{2}T Photonics). Both of these measurements are taken at point A shown in Fig. 4. The measured power of the transmitted DP-QPSK signal is $\sim$9.4 dBm and is attenuated to -20.6 dBm by the VOA, equaling a 150-km fiber transmission.

In the polarization separation and switching unit, the amplified and filtered DP-QPSK signal power is 0.2 dBm. The power of the two pumps are both set to be 18 dBm, and their wavelengths are tuned to be 1549.72 nm and 1550.12 nm, respectively. Figure 7 shows the generated optical spectrum of the FWM effect in the HNLF, measured at point B as shown in Fig. 4. The seven idler light beams are denoted as idler-1 to idler-7, corresponding to the different frequency mixtures listed in Table 1. A comparison is also made between these idler wavelengths and the ITU-T standard wavelengths. The idler wavelengths almost fit the ITU-T standard, but only idler-1 and idler-2 can be considered to be the results of polarization separation, because of our previous theoretical analysis (see Section 2). The power values of idler-1 and idler-2 are -10.2 dBm and -10.9 dBm respectively, with calculated conversion efficiencies of -10.4 dB and -11.1 dB, respectively.

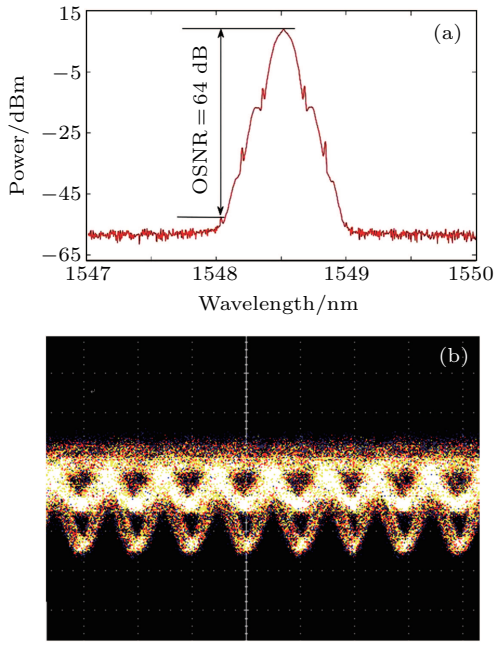


Fig. 6. Measured 100-Gbps DP-QPSK, showing (a) optical spectrum with 64-dB OSNR and (b) eye diagram (clear profile).

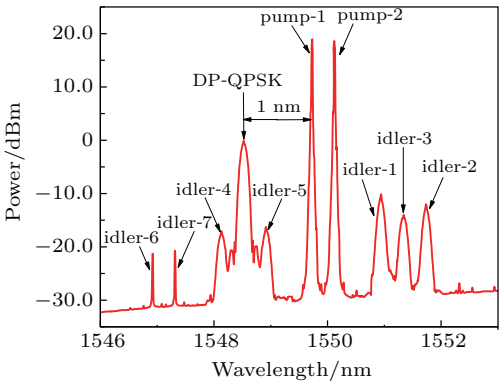


Fig. 7. FWM spectrum induced by a 100-Gbps DP-QPSK signal and two orthogonal polarization state pumps.

Table 1. Frequencies of idlers generated by the different FWM processes.

Number	Mixing frequency	Measured result/nm	ITU-T/nm	Deviation/nm	Suitable for Pol-separation
Idler-1	$2\omega_{p1}-\omega_s$	1550.931	1550.92	+0.011	√
Idler-2	$2\omega_{p2}-\omega_s$	1551.711	1551.72	−0.009	√
Idler-3	$\omega_{p1}+\omega_{p2}-\omega_s$	1551.315	1551.32	−0.005	×
Idler-4	$\omega_{p2}-\omega_{p2}+\omega_s$	1548.126	1548.12	+0.006	×
Idler-5	$\omega_{p2}-\omega_{p1}+\omega_s$	1548.914	1548.91	+0.004	×
Idler-6	$2\omega_2-\omega_{p2}$	1546.926	1546.92	+0.006	×
Idler-7	$2\omega_2-\omega_{p1}$	1547.313	1547.32	−0.007	×

In subsequent steps, the light beams of idler-1 and idler-2 are filtered by the DWDM module and sent to two receivers for signal recovery, based on coherent detection and offline DSP. Figure 8 shows the calculated demodulated constellation diagrams of the idler-1 (X-Pol) and idler-2 (Y-Pol) QPSK signals. The RMS EVMs of idler-1 and idler-2 are 14.32% and 14.11%, respectively; their calculated BERs are error-free. This fully explains that pump 1 only interacts with the X-Pol

component of the DP-QPSK signal to produce idler-1, while pump 2 only interact with the Y-Pol component to produce idler-2. Both of the two constellation diagrams in Fig. 8 are noticeably clear, implying that polarization separation based on orthogonally polarized FWM effect is successfully realized.

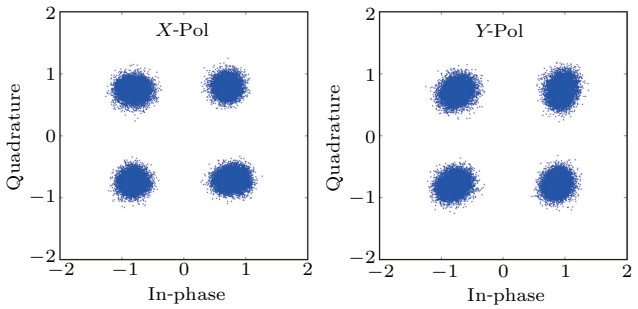


Fig. 8. Constellation diagrams of demodulated X-Pol and Y-Pol QPSK signals.

In order to obtain the most useful idler-1 and idler-2 light as the wavelength addresses, we shift the pump-1 and pump-2 wavelength simultaneously and measure the newly generated idler-1 and idler-2 power. To ensure the conversion power of idler is close to −15 dBm, a maximum spacing of 4 nm is adopted between the DP-QPSK signal and pump 1. Figures 9(a) and 9(b) show that the optical spectra of the pump-1 and pump-2 wavelengths shift to the right-hand side and left-hand side respectively, compared with Fig. 7. In the process of movement, the wavelength steps of pump 1 and pump 2 are adjusted at 0.2 nm (25 GHz). The generated idler-1 wavelengths can be selected in the ranges from 1540.56 nm to 1546.12 nm, and from the 1550.93 nm to 1556.53 nm, with a 0.4-nm grid. The idler-2 wavelengths, meanwhile, can be selected in ranges from 1539.75 nm to 1545.32 nm, and from 1551.72 nm to 1557.36 nm, again with a 0.4-nm grid. Figures 9(c) and 9(d) illustrate the measurements of all thirty available wavelength power values of idler-1 and idler-2 (right-hand side and left-hand side respectively). Both of the power values are distributed in a range from −10 dBm to −15 dBm, which supports the operation of error-free transmission.

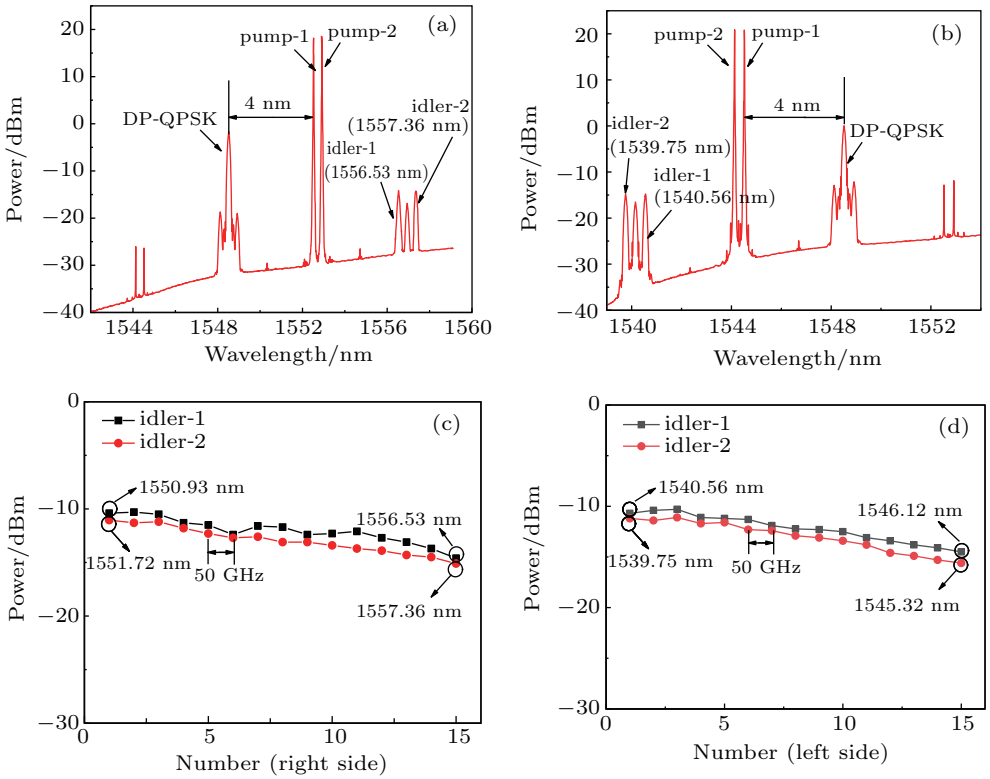


Fig. 9. FWM spectra of the pump-1 and pump-2 wavelengths shifted to (a) the right-hand side and (b) the left-hand side. All available measured idler-1 and idler-2 power are indicated on (c) right-hand side and (d) left-hand side, respectively.

To further evaluate the performance of the proposed system at a longer transmission distance, the BERs are measured by attenuating optical power through the VOA. Figure 10 shows the BERs, each as a function of the received power, for the two polarization separated idlers, alongside a BTB DP-QPSK signal shown for comparison. The received power is measured at point B as shown in Fig. 4. As shown in Fig. 10, the required powers for idler-1 and idler-2 (with a data rate of 50 Gbps) are −36.84 dBm and −36.28 dBm respectively, at a BER of 3.8×10^{-3}. The required power values for the X- and Y-polarization states of the BTB DP-QPSK are −41.61 dBm and −41.23 dBm, respectively. Therefore, the power penalties in the polarization separation process, caused by noise introduced into the conversion process such as amplifier noise and vector FWM, are 4.77 dB for the X-polarization state and 4.95 dB for the Y-polarization state.

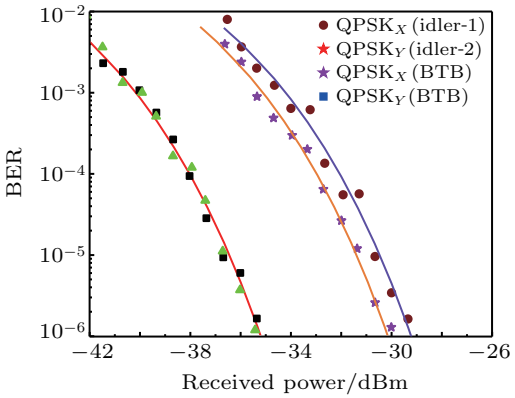


Fig. 10. Measured BERs each as a function of received power for two polarization demultiplexed idlers and BTB signals.

5. Conclusions

In this work, we analyze a novel scheme to achieve simultaneous polarization separation and switching for an ultra-high-speed Pol-MUX fiber network, both theoretically and experimentally, by using the orthogonally-polarized FWM effect. The two orthogonal polarization states of a 100-Gbps DP-QPSK signal are separated into two independent channels with different wavelengths; these two polarization separated QPSK signals have clear constellation diagrams with RMS EVMs of 14.32% and 14.11% respectively. The wavelength of the idlers can be generated at 30 different ITU-T wavelengths by easily changing the pump wavelength, and the power values of these idlers are in a range between −10 dBm and −15 dBm, indicating that they can support error-free transmission. The power penalty, is 5 dB lower than that of BTB signal for both the X- and Y-polarization components, measured at a BER of 3.8×10^{-3}. Based on the results presented above, our novel scheme can provide a simultaneous polarization separation and switching method that could be applied to future backbone networks.

References

[1] Winzer P and Essiambre R J 2006 *J. Lightwave Technol.* **24** 4711
[2] Pfeiffer T 2015 *J. Opt. Commun.* **7** B38
[3] Lam C F, Liu H, Koley B, Zhao X X, V K and V G 2010 *IEEE Commun. Mag.* **48** 32
[4] Tan M, Rosa P, Le S T, Phillips L D and Harper P 2015 *Opt. Express* **23** 22181
[5] Khanna G, Rahman T, Man E D and Riccardi E 2016 *IEEE Photon. Technol. Lett.* **29** 189
[6] Xu T, Shevchenko N, Lavery D, Semrau D, Liga G, Alvarado A, Killey R and Bayvel P 2017 *Opt. Express* **25** 3311
[7] Zhang Z Y, Jiang W R, Wang B, Yang Y Q and Wang Z G 2018 *Chin. Phys. B* **27** 013102
[8] Pan Y, Yan L S, Yi A L, Ji. L, Pan W, Luo B and Zou X H 2017 *Opt. Lett.* **42** 4071
[9] Chen Z Y, Yan L S, Pan Y, Jiang L, Yi A L, Pan W and Luo B 2017 *Light: Science & Applications* **6** e16207
[10] Ji H C, Lee J H, Kim H, Park P J and Chung Y C 2009 *Opt. Express* **17** 1169
[11] Steve X, Yan L S, Zhang B, Willner A E and Jiang J F 2007 *Opt. Express* **15** 7407
[12] Koch B, Noe R, Sandel D, Mirvoda V and Omar J 2013 *IEEE Photon. Technol. Lett.* **25** 798
[13] Xu F, Guo M Q, Wang L Qiao Y J and Tian H P 2016 *Chin. Phys. B* **25** 084208
[14] Tian F, Zhang X G, Weng X, Xi L X, Zhang Y A and Zhang W B 2011 *Chin. Phys. B* **20** 080702
[15] Gerstel O, Jinno M, Lord A and Ben S J 2012 *IEEE Commun. Mag.* **50** s12
[16] Kachris C and Tomkos L 2012 *IEEE Commun. Surveys & Tutorials* **14** 1021
[17] Kameda Y, Hashimoto Y and Yorozu S 2008 *IEICE Trans. Electron* **E91-C** 333
[18] Hoang T M, Osman M M, Chagnon M, Qiu M and Patel D 2015 *Opt. Commun.* **356** 269
[19] Cuik S, Xia W J, Shang J, Ke C J, Fu S N and Liu D M 2016 *Opt. Commun.* **366** 200
[20] Papadimitriou G, Papazoglou C and Pomportsis A S 2003 *J. Lightwave Technol.* **21** 384
[21] Wang Y and Cao X J 2011 *IEEE Communications Surveys & Tutorials.* **14** 698
[22] Wen Y H and Feng K M 2015 *IEEE Photon. Technol. Lett.* **27** 935
[23] Anthur A P, Zhou R, Duill S O, Walsh A J, Martin E, Venkitesh D and Barry L P 2016 *Opt. Express* **24** 11749
[24] Lin Q and Agrawal G P 2004 *Opt. Lett.* **29** 1114
[25] Ma J X, Yu J J, Yu C X and Zhou Z 2006 *Opt. Commun.* **260** 522
[26] Uzunidis D, Matrakidis C and Stavdas A 2016 *Opt. Commun.* **378** 22
[27] Mateo E, Zhu L K and Li G F 2008 *Opt. Express* **16** 16124
[28] Radic S, Mckinstrie C J, Jopson R M, Centanni J C and Chraplyvy A R 2003 *IEEE Photon. Technol. Lett.* **15** 957
[29] Cui Y D, Lu F F and Liu X M 2017 *Sci. Rep.* **7** 40080
[30] Wang T, Niu M S, Bu M M, Han P G, Hao D Z, Yang J S and Song L K 2018 *Acta Phys. Sin.* **67** 100701 (in Chinese)
[31] Li P, Wu D J, Liu S, Zhang Y, Guo X Y, Qi S X, Li Y and Zhao J L 2017 *Chin. Phys. B* **26** 114201
[32] Wang Z N and Xie C J 2009 *Opt. Express* **17** 3183
[33] Koch B, Noe R, Mirvoda V, Griesser H, Bayer S and Wernz H 2010 *IEEE Photon. Technol. Lett.* **22** 1407